

Article

Open Access



# A low-concentration sulfone electrolyte enables high-voltage chemistry of lithium-ion batteries

Ling Lv<sup>1</sup>, Haikuo Zhang<sup>1</sup>, Di Lu<sup>1</sup>, Yuan Yu<sup>2,\*</sup>, Jiacheng Qi<sup>1</sup>, Junbo Zhang<sup>1</sup>, Shuoqing Zhang<sup>1</sup>, Ruhong Li<sup>1</sup>, Tao Deng<sup>3</sup>, Lixin Chen<sup>1,4</sup>, Xiulin Fan<sup>1,\*</sup>

<sup>1</sup>State Key Laboratory of Silicon Materials, School of Materials Science and Engineering, Zhejiang University, Hangzhou 310027, Zhejiang, China.

<sup>2</sup>Zhejiang Provincial Key Laboratory of Fiber Materials and Manufacturing Technology, Zhejiang Sci-Tech University, Hangzhou 310018, Zhejiang, China.

<sup>3</sup>Department of Chemical and Biomolecular Engineering, University of Maryland, College Park, MD 20742, USA.

<sup>4</sup>Key Laboratory of Advanced Materials and Applications for Batteries of Zhejiang Province, Hangzhou 310013, Zhejiang, China.

\***Correspondence to:** Dr. Xiulin Fan, State Key Laboratory of Silicon Materials, School of Materials Science and Engineering, Zhejiang University, Hangzhou 310027, Zhejiang, China. E-mail: xlfan@zju.edu.cn; Dr. Yuan Yu, Zhejiang Provincial Key Laboratory of Fiber Materials and Manufacturing Technology, Zhejiang Sci-Tech University, Hangzhou 310018, Zhejiang, China. E-mail: yuyu@zstu.edu.cn

**How to cite this article:** Lv L, Zhang H, Lu D, Yu Y, Qi J, Zhang J, Zhang S, Li R, Deng T, Chen L, Fan X. A low-concentration sulfone electrolyte enables high-voltage chemistry of lithium-ion batteries. *Energy Mater* 2022;2:200030. <https://dx.doi.org/10.20517/energymater.2022.38>

**Received:** 11 Jul 2022 **First Decision:** 5 Aug 2022 **Revised:** 5 Aug 2022 **Accepted:** 10 Aug 2022 **Published:** 25 Aug 2022

**Academic Editors:** Yuping Wu, Hong Xu **Copy Editor:** Tiantian Shi **Production Editor:** Tiantian Shi

## Abstract

Commercial carbonate electrolytes with poor oxidation stability and high flammability limit the operating voltage of Li-ion batteries (LIBs) to ~4.3 V. As one of the most promising candidates for electrolyte solvents, sulfolane (SL) has received significant interest because of its wide electrochemical window, low flammability and high dielectric permittivity. Unfortunately, SL-based electrolytes with normal concentrations cannot achieve highly reversible Li<sup>+</sup> intercalation/deintercalation in graphite anodes due to an ineffective solid electrolyte interface, thus undermining their potential application in LIBs. Here, a low-concentration SL-based electrolyte (LSLE) is developed for high-voltage graphite||LiNi<sub>0.8</sub>Co<sub>0.1</sub>Mn<sub>0.1</sub>O<sub>2</sub> (NCM811) full cells. A highly reversible graphite anode can be achieved through the preferential decomposition of the dual-salt LiDFOB-LiBF<sub>4</sub> in the LSLE. The addition of fluorobenzene further restrains the decomposition of SL, endowing uniform, robust and inorganic-rich interphases on the electrode surfaces. As a result, the LSLE with improved thermal stability can support the MCMB||NCM811 full cells at 4.4 V, evidenced by an excellent cycling performance with capacity retentions of 83% after 500 cycles at 25 °C and 82% after 400 cycles at 60 °C. We believe that the design of this fluorobenzene-containing LSLE offers an effective routine for next-generation low-cost and safe electrolytes for high-voltage LIBs.



© The Author(s) 2022. **Open Access** This article is licensed under a Creative Commons Attribution 4.0 International License (<https://creativecommons.org/licenses/by/4.0/>), which permits unrestricted use, sharing, adaptation, distribution and reproduction in any medium or format, for any purpose, even commercially, as long as you give appropriate credit to the original author(s) and the source, provide a link to the Creative Commons license, and indicate if changes were made.



**Keywords:** Electrolyte, sulfone, fluorobenzene, interphase, lithium-ion batteries (LIBs)

## INTRODUCTION

Lithium-ion batteries (LIBs) have achieved tremendous success in portable electronic devices, electric vehicles and various power grid applications owing to their high energy and power densities and long cycle life<sup>[1-3]</sup>. To further increase the energy density of LIBs, high-voltage cathodes, including Li-rich layered oxides ( $\text{Li}_{1-x}\text{M}_{1-x}\text{O}_2$ ,  $\text{M} = \text{Mn, Ni or Co}$ ) and Ni-rich layered oxides ( $\text{LiNi}_{1-x-y}\text{Co}_x\text{Mn}_y\text{O}_2$ ,  $1-x-y \geq 0.6$ ) have been intensively explored and shown some progress<sup>[4,5]</sup>. However, the electrochemical performance of these aggressive cathodes is critically hindered by commercial carbonate electrolytes, which are responsible for the high flammability and continuous decomposition above 4.3 V vs.  $\text{Li}^+/\text{Li}$ <sup>[6,7]</sup>. The undesired decomposed products, including alkyl alcohols (ROH) and carbonates ( $\text{ROCO}_2\text{H}$ ), are detrimental to the formation of a stable cathode electrolyte interphase (CEI)/solid electrolyte interphase (SEI)<sup>[8]</sup>. In addition,  $\text{LiPF}_6$  with poor thermal stability and high susceptibility to moisture is prone to the generation of pernicious byproducts, including phosphorus pentafluoride ( $\text{PF}_5$ ) and hydrogen fluoride (HF)<sup>[9,10]</sup>, which accelerate the dissolution of transition metal (TM) ions from the cathodes, thus destroying their structure and decreasing the reversible capacity<sup>[11-13]</sup>. Therefore, it is necessary and urgent to develop novel electrolytes with wide electrochemical windows, non-/low flammability and good compatibility with graphite and aggressive cathodes<sup>[14-16]</sup>.

A number of non-carbonate electrolytes (e.g., nitriles<sup>[17-19]</sup>, sulfones<sup>[20-22]</sup>, ionic liquids<sup>[23-25]</sup> and fluorinated electrolytes<sup>[26-30]</sup>) with excellent anodic stability have been widely explored recently. Among them, sulfolane (SL) stands out with the distinct merits of a high dielectric constant (43.4 at 303.2 K), low flammability, high flash point ( $T_f = 166\text{ }^\circ\text{C}$ ), high boiling point ( $T_b = 287\text{ }^\circ\text{C}$ ) and wide electrochemical window ( $> 5\text{ V vs. Li/Li}^+$ )<sup>[22,31]</sup>. The most effective strategy to enable SL electrolyte-based LIBs is to increase the salt ratio to form highly concentrated electrolytes (HCEs)<sup>[32-34]</sup>, which improve the compatibility with graphite by forming an anion-dominated SEI. The method of HCEs inevitably results in high viscosity and cost and low  $\text{Li}^+$  ionic conductivity. In this regard, there is an urgent need for appropriate strategies to design low-concentration SL to support commercial battery chemistries.

In this study, we report a novel dual-salt design with a co-solvent of fluorobenzene (FB) to functionalize a low-concentration SL electrolyte with good thermal stability and capability to enable a highly reversible graphite anode and Ni-rich layer cathode  $\text{LiNi}_{0.8}\text{Co}_{0.1}\text{Mn}_{0.1}\text{O}_2$  (NCM811). The rationally designed electrolyte consists of 0.8 M LiDFOB and 0.2 M  $\text{LiBF}_4$  in a mixture of SL/FB (2.8:1 by vol.), denoted as LiDFOB- $\text{LiBF}_4$ /SL-FB. Compared with  $\text{LiPF}_6$ ,  $\text{LiBF}_4$  exhibits many advantages, including satisfactory thermal stability, relatively low moisture sensitivity and small charge transfer resistance<sup>[35,36]</sup>; however, the formation of an erratic SEI on the surface of graphite has been a major challenge for its application in LIBs<sup>[37]</sup>. In contrast, LiDFOB has been explored mostly as a lithium salt and functional additive due to its excellent film-forming ability<sup>[38,39]</sup>, benign thermal stability (up to  $240\text{ }^\circ\text{C}$ ) and passivation performance to aluminum collectors<sup>[40,41]</sup>. Hence, the combination of LiDFOB with a dose of  $\text{LiBF}_4$  can be an effective solution to improve the performance of SL by overcoming the intractable issues of incompatibility with the graphite anode at normal salt concentrations. The presence of FB in the electrolyte provides additional advantages, such as low viscosity and density and reasonable stability at high voltages<sup>[42]</sup>. The dual-salt and FB are preferentially decomposed to generate a homogeneous, thin and robust SEI/CEI mainly composed of LiF and a small amount of sulfur-containing species on the surfaces of both the graphite anode and NCM811 cathode. As a result, the designed LSLE significantly promotes the cycling performance of high-voltage MCMB||NCM811 full cells, as evidenced by an 83% retention after 500 cycles, unprecedented rate performance ( $169.9\text{ mAh g}^{-1}$

at 5C) and impressive elevated temperature performance (82% capacity retention after 400 cycles at 60 °C). The present study provides a remarkable and efficient strategy for designing LSLEs to cater to aggressive NCM811 cathodes and address the incompatibility with graphite, thereby providing novel directions in electrolyte design.

## EXPERIMENTAL

### Materials

Lithium metal foil was purchased from Tianjin China Energy Lithium Co., Ltd. NCM811 powder, MCMB powder and conductive carbon black (Super C45) were purchased from Hefei Kejing Materials Technology Co., Ltd. Poly(vinylidene fluoride) (PVDF) binder, LA133, N-methylpyrrolidone (NMP), dimethyl carbonate (DMC), ethylene carbonate (EC) and SL were purchased from Duoduo Chem Co., Ltd. FB was purchased from Macklin Co., Ltd. LiDFOB, LiBF<sub>4</sub> and LiPF<sub>6</sub> were purchased from Dadu New Material Co., Ltd. All lithium salts and solvents were of battery grade.

### Preparation of electrodes, electrolytes and cells

The cathode slurry contained 80 wt.% NCM811, 10 wt.% Super C45, 10 wt.% PVDF and NMP as a solvent. The resulting slurry was coated on Al foil. The anode slurry contained 93 wt.% MCMB, 2 wt.% Super C45, 5 wt.% LA133 and pure H<sub>2</sub>O as a solvent. The resulting slurry was coated on Cu foil. After solvent drying, the electrodes were further dried at 100 °C for 12 h under a vacuum. The electrodes were then punched into disks with diameters of 14 and 12 mm for anodes and cathodes, respectively. The mass loadings of MCMB and NCM811 electrodes for coin cells were ~6.7 and ~6.6 mg cm<sup>-2</sup>, respectively. The two reference electrolytes were 1 M LiPF<sub>6</sub>/EC-DMC (1:1 v/v) (labelled as BE) and 0.8 M LiDFOB-0.2 M LiBF<sub>4</sub> in SL (labelled as LiDFOB-LiBF<sub>4</sub>/SL). The LSLE was prepared by mixing 0.8 M LiDFOB and 0.2 M LiBF<sub>4</sub> with SL/FB (2.8:1, v/v). All solvents were dried using molecular sieves and the preparation of all the electrolytes was performed in a glovebox with an argon atmosphere (< 0.1 ppm of O<sub>2</sub> and H<sub>2</sub>O) (Mikrouna, China). We used one polyethylene separator and one glass fiber separator between the anode and cathode inside the coin cells with 100 μL of electrolyte. MCMB||NCM811 full cells were prepared in CR2025 coin-type cells with a set N/P value of 1.2 (calculated according to 320.0 mAh g<sup>-1</sup> for MCMB and 200.0 mAh g<sup>-1</sup> for NCM811). AG||NMC811 pouch-type cells (1 Ah) were purchased from LI-FUN Technology Co., Ltd.

### Electrochemical tests

Coin cells were charged and discharged in calorstats using a LAND battery testing system (Wuhan LAND Electronics Co., Ltd.). MCMB||NCM811 full cells were activated at a rate of 0.1C for two cycles and then operated at 0.5C for long cycling with a cutoff voltage between 4.4/4.3 and 2.8 V. Li||MCMB half-cells were operated at a rate of 0.1C at a potential range of 0.005-1.5 V. The rate capability was obtained from MCMB||NMC811 full cells cycled at constant charge (0.2C) and different discharge rates (0.5C, 1C, 2C, 3C, 4C and 5C). The AG||NMC811 (1 Ah) pouch-type cells were cycled at a 0.1C rate for two formation cycles and then 0.3C charge/discharge for long cycling under 2.8-4.3 V. Linear sweep voltammetry (LSV) was performed using an electrochemical workstation (Ivium-n-stat, Ivium Technologies BV Co., Ltd.) in a coin cell with lithium foil as a working electrode and stainless steel as counter and reference electrodes at a scanning rate of 0.5 mV/s. Electrochemical impedance spectroscopy (EIS) measurements of the MCMB||NCM811 full cells at a fully discharged state were also performed using the same electrochemical workstation over frequencies from 10 kHz to 0.01 Hz.

### Characterization

The electrodes disassembled from MCMB||NCM811 full cells were washed with DMC before subsequent characterization to prevent any disturbance from the residual salts. X-ray diffraction (XRD, X-pert Powder, PANalytical B.V.) was performed with Cu K $\alpha$  radiation from 5° to 80° at a scanning speed of 4° min<sup>-1</sup>.

Scanning electron microscopy (SEM, SU-70, Hitachi Ltd.) was carried out to observe the morphology of the electrodes. The microstructures of the SEI/CEI were obtained from transmission electron microscopy (TEM, Tecnai G2 F20). X-ray photoelectron spectroscopy (XPS, Escalab 250Xi, Thermo Fisher Scientific) was used to observe the composition of the interphases. For the TM ion dissolution study using inductively coupled plasma mass spectrometry (ICP-MS, Agilent 7700) on cycled NCM811 cathodes, samples were fully charged and disassembled from MCMB||NCM811 full cells after 50 cycles. For the DSC experiments, the Li||NCM811 half-cells fabricated with each electrolyte (100  $\mu$ L) were fully charged to 4.4 V at 0.1C and maintained for 20 h. Approximately 3.0 mg of samples and 10  $\mu$ L of electrolytes were hermetically sealed in a pan, respectively. The temperature was increased from ambient to 300  $^{\circ}$ C at a heating rate of 5  $^{\circ}$ C  $\text{min}^{-1}$ .

### Theoretical calculations

Density functional theory (DFT) calculations using Gaussian 09 software were used to carry out the molecular optimization. Using the three-parameter empirical formulation B3LYP in conjunction with the basis set of 6-311+G (d, p), the highest occupied molecular orbital (HOMO) and lowest unoccupied molecular orbital (LUMO) were observed. Ab initio molecular dynamics (AIMD) calculations were performed using the Vienna Ab initio Simulation Package<sup>[43-45]</sup>. By positioning LiDFOB, LiBF<sub>4</sub>, SL and FB in a box based on density and molar ratio, we constructed an electrolyte system for the simulations. All AIMD calculations were performed using the NVT ensemble with a Nosé-Hoover thermostat at 300 K. A time step of 1 fs and only the Gamma point in the reciprocal space were used in our calculations. The total simulation time was 10 ps. The projected density of states (DOS) was calculated to observe the distribution of the LUMO level. H transfer energies were calculated by positioning different solvents onto the charged NCM811 surface with a cutoff energy of 550 eV.

## RESULTS AND DISCUSSION

The LUMO and HOMO are key indicators of salt and solvent stability. As can be seen from [Figure 1A](#), LiDFOB has the lowest LUMO value (-2.80 eV) among all the electrolyte components, indicating that it tends to be decomposed first, which is in good agreement with the outstanding film-forming ability reported in previous studies<sup>[46,47]</sup>. LiBF<sub>4</sub> (-1.5 eV) and FB (-0.84 eV) with less negative LUMOs than LiDFOB are able to mature the nascent LiDFOB-derived SEI. In addition, the DOS shows that the LUMO is mainly located at the LiDFOB and LiBF<sub>4</sub> molecules in the 0.8 M LiDFOB-0.2 M LiBF<sub>4</sub>/SL (denoted as LiDFOB-LiBF<sub>4</sub>/SL) electrolyte [[Supplementary Figure 1](#)], implying the preferential reduction of LiDFOB and LiBF<sub>4</sub> within the electrolyte. With the presence of FB, the LUMO level of the electrolyte emerges on FB rather than SL [[Figure 1B](#)], suggesting that both the dual-salt and FB contribute to the SEI formation, which suppresses the reactivity of SL in the following cycles. The electrostatic potential (ESP) in [Figure 1C](#) depicts that the  $E_{\text{min}}$  value of SL (-40.94 kcal mol<sup>-1</sup>) is much lower than that of FB (-19.19 kcal mol<sup>-1</sup>), which demonstrates the involvement of SL rather than FB in the solvation of Li<sup>+</sup>. The result is further confirmed by the snapshots of the AIMD simulation [[Figure 1D](#) and [Supplementary Figure 2A](#)]. The radical distribution function reveals that the first coordinated shell of Li<sup>+</sup> (within 2 Å) is dominated by SL molecules, whereas the number of FB molecules in the inner solvation shell of Li<sup>+</sup> is negligible [[Figure 1E](#) and [Supplementary Figure 2B](#)], in agreement with the ESP results. Guided by the above results, we portray the decomposition order of components in the SL-based electrolyte with reduction potentials schematically in [Figure 1F](#) and [Supplementary Figure 3](#). The brittle SEI generated by the preferential decomposition of the dual-salt is not sufficient to block the continuous decomposition of SL, whereas the addition of FB can further effectively form a protective interface, which restricts the continual reduction of SL without changing the solvation structure.

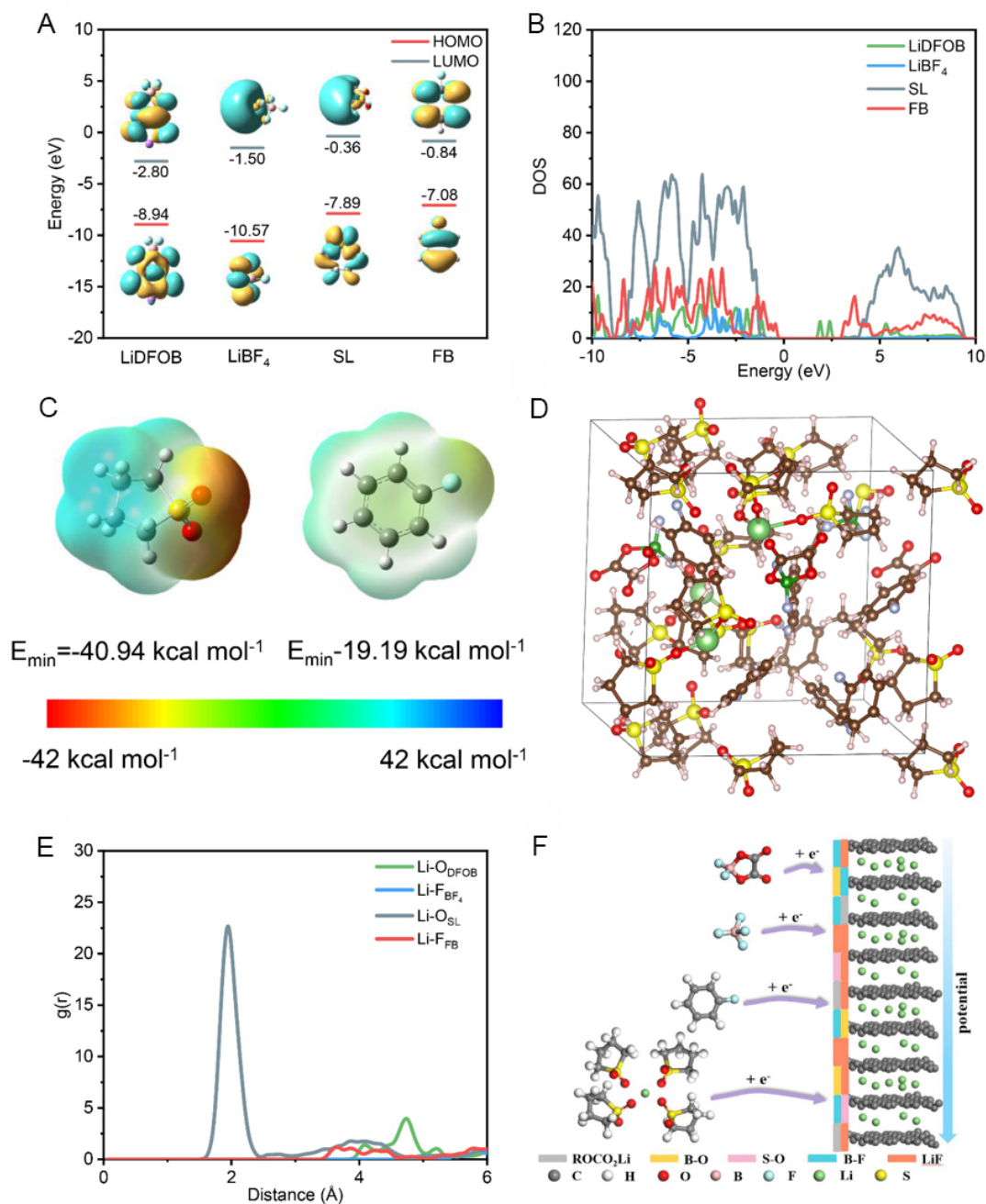


**Figure 1.** (A) Frontier molecular orbital energies of LiDFOB, LiBF<sub>4</sub>, SL and FB, together with their molecular orbital diagrams. (B) DOS obtained from AIMD simulations of LiDFOB-LiBF<sub>4</sub>/SL-FB. (C) Electrostatic potential diagrams of SL and FB. (D) AIMD simulation snapshots of LiDFOB-LiBF<sub>4</sub>/SL-FB (brown: C atom, white: H atom, red: O atom, green: Li atom, yellow: S atom, silver: F atom and dark green: B atom). (E) Radial distribution functions of Li-O<sub>DFOB</sub>, Li-F<sub>BF<sub>4</sub></sub>, Li-O<sub>SL</sub> and Li-F<sub>FB</sub> pairs calculated from AIMD simulation trajectories in LiDFOB-LiBF<sub>4</sub>/SL-FB electrolyte. (F) Schematic diagram of reactions at LiDFOB-LiBF<sub>4</sub>/SL-FB electrolyte/graphite interphase.

Apart from the ability to construct a robust interface, FB also significantly lowers the viscosity of the SL-based electrolyte [Supplementary Figure 4], which greatly accelerates the electrolyte infiltration and promotes Li<sup>+</sup> transport within the electrodes. The oxidation stability of the LiDFOB-LiBF<sub>4</sub>/SL-FB electrolyte evaluated by LSV is up to 5.0 V (vs. Li/Li<sup>+</sup>) [Figure 2A]. Furthermore, the Li||NCM811 cell with LiDFOB-

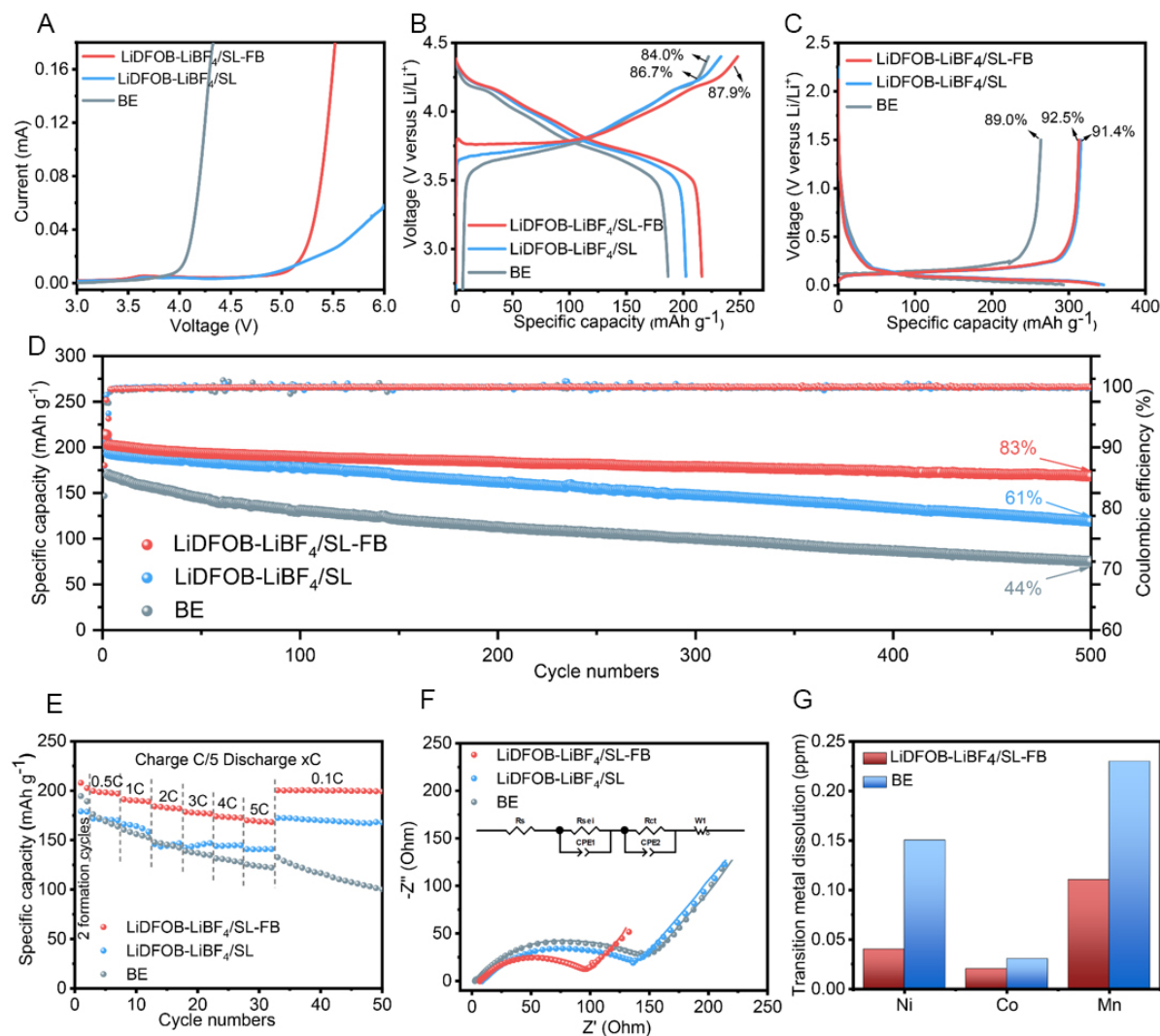


**Figure 2.** (A) LSV profiles of Li||stainless steel cells with various electrolytes at a rate of 0.5 mV/s. (B) Initial charge-discharge voltage curves of Li||NCM811 half-cells and (C) Li||MCMB half-cells using different electrolytes. (D) Cycling performance and Coulombic efficiency vs. cycle number of MCMB||NCM811 full cells with various electrolytes at 0.5C between 2.8 and 4.4 V at 25 °C. (E) Rate capacity of MCMB||NCM811 full cells with various electrolytes under varying discharge rates (x)C (1C = 200 mA g<sup>-1</sup>) and the same charge rate (C/5) at 2.8–4.4 V. (F) EIS measurements of MCMB||NMC811 full cells after 100 cycles. (G) TM dissolution measured by ICP-MS after 50 cycles with various electrolytes.

LiBF<sub>4</sub>/SL-FB exhibits a higher initial Coulombic efficiency of 87.9% [Figure 2B] than that of the reference electrolytes [86.7% for LiDFOB-LiBF<sub>4</sub>/SL and 84.0% for 1 M LiPF<sub>6</sub>/EC-DMC (denoted as BE)], suggesting that the designed LSLE can build a more robust surface passivation layer on NCM811 and ensure high oxidation stability. Furthermore, the compatibility of the SL-based electrolyte with the graphite anode was tested using Li||MCMB cells. As shown in Figure 2C, the highest initial Coulombic efficiency of 92.5% with the LiDFOB-LiBF<sub>4</sub>/SL-FB electrolyte (91.4% for LiDFOB-LiBF<sub>4</sub>/SL and 89.0% for BE) indicates that the dual-salt with good film-forming capability can successfully address the incompatibility of the SL-based electrolyte towards graphite at low concentrations. In addition, FB facilitates the cycling stability of the SL-based electrolyte [Supplementary Figure 5]. The capacity retention of the Li||MCMB half-cell with BE declines to 93% after 100 cycles, while the Coulombic efficiency of the Li||MCMB half-cell with LiDFOB-LiBF<sub>4</sub>/SL fluctuates slightly. In sharp contrast, no capacity fading is detected for the Li||MCMB half-cell with

the LiDFOB-LiBF<sub>4</sub>/SL-FB electrolyte after 100 cycles, suggesting that the dual-salt at low concentrations makes the SL-based electrolyte effective against graphite. The addition of FB further optimizes the interface on the graphite and suppresses the subsequent decomposition of SL.

The cycling behavior of the MCMB||NCM811 full cells using different electrolytes were investigated [Figure 2D]. A low capacity retention of only 44% (75.1 mAh g<sup>-1</sup>/170.3 mAh g<sup>-1</sup>) can be obtained after 500 cycles for the cell with BE due to the formation of a poor CEI on the NCM811 cathode and serious parasitic reactions. Benefitting from the synergistic effect of the dual-salt, the performance of the MCMB||NCM811 cell using the LiDFOB-LiBF<sub>4</sub>/SL electrolyte can be significantly improved, yet there is still a drastic capacity fade with 61% of the initial capacity (118.5/193.5 mAh g<sup>-1</sup>) retained within 500 cycles. After adding FB, the MCMB||NCM811 cell presents the best electrochemical performance with a higher initial discharge capacity (214.1 mAh g<sup>-1</sup>) than reference electrolytes (204.3 mAh g<sup>-1</sup> for BE and 208.3 mAh g<sup>-1</sup> for LiDFOB-LiBF<sub>4</sub>/SL). Impressively, the MCMB||NCM811 cell with the FB-containing LSLE shows high Coulombic efficiency (99.9%) and a significantly enhanced capacity retention of 83% (168.5 mAh g<sup>-1</sup>/202.6 mAh g<sup>-1</sup>) after 500 cycles [Supplementary Figure 6].

In addition to the remarkable cycling stability, the rate performance of the MCMB||NCM811 cell in the LiDFOB-LiBF<sub>4</sub>/SL-FB electrolyte is also superior to that of the reference electrolytes. Under a current density of 5C (1C = 200 mA g<sup>-1</sup>), the cell with the LiDFOB-LiBF<sub>4</sub>/SL-FB electrolyte achieves a high reversible capacity of 169.9 mAh g<sup>-1</sup> [Figure 2E and Supplementary Figure 7], while the cells with LiDFOB-LiBF<sub>4</sub>/SL and BE electrolytes deliver limited capacities of 140.9 and 125.5 mAh g<sup>-1</sup>, respectively. When the rate is set back to 0.1C, the cell with the LSLE presents a higher reversible discharge capacity of 200.3 mAh g<sup>-1</sup> (172.4 mAh g<sup>-1</sup> for LiDFOB-LiBF<sub>4</sub>/SL and 132.6 mAh g<sup>-1</sup> for BE). EIS was conducted on the MCMB||NCM811 cells to study the capacity degradation mechanism [Supplementary Table 1]. The semicircles in the high- ( $R_{SEI}$ ) and medium-frequency ( $R_{ct}$ ) regions of the Nyquist plots represent the resistance of the electrode/electrolyte interphase ( $R_i$ )<sup>[48]</sup>. As shown in Figure 2F and Supplementary Figure 8, the introduction of FB significantly decreases the interphase resistance to 103.1 Ohm after 100 cycles, compared with 128.4 Ohm for LiDFOB-LiBF<sub>4</sub>/SL and 145.8 Ohm for BE. The above results illustrate that the combination of dual-salts and FB improves the electrode/electrolyte interface by preventing continual side reactions and improving Li<sup>+</sup> diffusion. Such an interface is also conducive to reducing the dissolution of TM ions<sup>[49]</sup>, and the Mn/Ni contents of the cycled NMC811 in the LSLE are reduced two- and threefold compared with those in BE, respectively [Figure 2G].

To further elucidate the reactions of LiDFOB-LiBF<sub>4</sub>/SL-FB on the electrolyte/electrode interphase, DFT and post-mortem characterization were conducted. Basically, solvent oxidation on the highly delithiated NCM811 surface is dominated by H transfer and the discernibly different energy of the H transfer reaction determines the oxidation stability of the electrolytes. The dehydrogenation energy of isolated SL ( $\Delta E_{SL} = 1.17$  eV) is much more positive than FB ( $\Delta E_{FB} = -2.11$  eV), EC ( $\Delta E_{EC} = -2.61$  eV) and DMC ( $\Delta E_{DMC} = -0.83$  eV) [Figure 3A-C and Supplementary Figure 9], suggesting a higher oxidation stability for the SL molecule, which agrees well with the LSV results. No significant difference between the pristine NCM811 and cycled NCM811 cathodes are detected in the XRD patterns [Supplementary Figure 10], indicating that the cycling with the three electrolytes has no effect on the bulk structure of the NCM811 cathodes, while the stability of the electrode/electrolyte interphase is a key factor to determine the battery performance. As shown in Supplementary Figure 11A, the SEM images of the pristine NCM cathode are presented in the form of spherical aggregates, and the NCM811 particle surfaces are clean, smooth and flat. After cycling in BE and the LiDFOB-LiBF<sub>4</sub>/SL electrolyte, serious cracks and substantial decomposition products are found on the NMC811 particle surfaces [Supplementary Figures 11B and C]. Fortunately, the NCM811 cathode

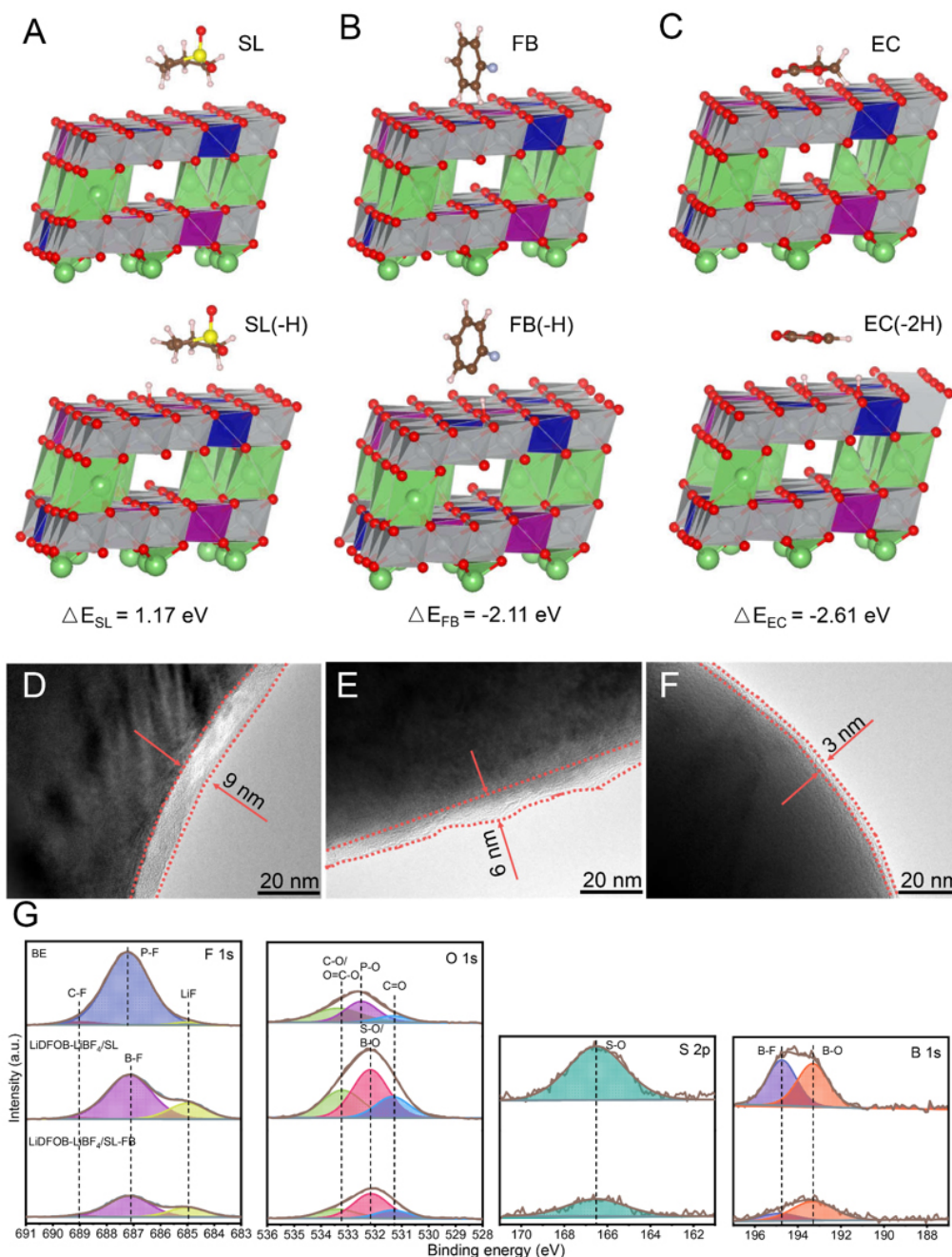


**Figure 3.** H-transfer reaction from (A) SL/SL (-H), (B) FB/FB (-H) and (C) EC/EC(-2H) to the delithiated NCM811 (003) cathode surface from periodic DFT calculations. Typical HR-TEM images of cycled NCM811 electrodes recovered from MCMB||NCM811 full-cells after 50 cycles with (D) BE, (E) LiDFOB-LiBF<sub>4</sub>/SL and (F) LiDFOB-LiBF<sub>4</sub>/SL-FB. (G) XPS F 1s, O 1s, S 2p and B 1s spectra for NCM811 cathodes recovered from MCMB||NCM811 full cells after 50 cycles with various electrolytes.

particles cycling in LiDFOB-LiBF<sub>4</sub>/SL-FB almost maintain their original morphology without discernible damage [Supplementary Figure 11D]. More solid evidence of the effective cathode protection in the FB-containing SL-based electrolyte can be obtained from high-resolution transmission electron microscopy (HR-TEM). A non-uniform CEI layer with a thickness of 9 nm is formed on the NCM811 particles because of the continual oxidation of the BE electrolyte on the catalytic surfaces [Figure 3D], which is detrimental to

the Li<sup>+</sup> transport, resulting in kinetic issues and an irreversible capacity loss. Although improvements are obtained by the participation of the dual-salt in the CEI formation, a thick and irregular interface (6 nm) is formed due to the decomposition of SL in LiDFOB-LiBF<sub>4</sub>/SL [Figure 3E]. With the addition of FB, the CEI formed in the optimized SL-based electrolyte is discernibly decreased to 3 nm with a uniform morphology [Figure 3F]. These results prove that FB and the dual-salt at a low concentration effectively restrain the decomposition of SL, resulting in a thin and dense passivation layer on the NCM811 particles.

XPS was carried out to unveil the compositional information of the interphases on NCM811. In the C 1s spectrum, the peaks at 286.0 eV (C-C), 287.3 eV (C-O) and 289.1 eV (C=O) and 290.6 eV (O=C-O) originate from the decomposed by-products (ROH, ROCO<sub>2</sub>H and so on) of the electrolyte [Supplementary Figure 12], in line with the results for the O 1s spectrum [Figure 3G]. The content of S-O (532.1 eV, O 1s and 166.5 eV, S 2p) in the FB-containing SL-based electrolyte is significantly lower than that of LiDFOB-LiBF<sub>4</sub>/SL, implying a more protective CEI derived from FB and the dual-salt to eschew the decomposition of SL. The F 1s and P 2p spectra show that the CEI formed in BE is rich in P-F and P-O due to the by-products (Li<sub>x</sub>PO<sub>y</sub>F<sub>z</sub> and Li<sub>x</sub>PF<sub>y</sub>) of LiPF<sub>6</sub> decomposition. Furthermore, the SEI formed in the optimized SL-based electrolyte has a weaker LiF peak than that in LiDFOB-LiBF<sub>4</sub>/SL, which is beneficial in reducing the impedance of the CEI and facilitating Li<sup>+</sup> diffusion<sup>[50]</sup>. Therefore, we can tentatively conclude that the interphase generated by the FB-containing LSLE is mainly composed of sulfur-containing species and LiF, originating from the decomposition of FB and the dual-salt rather than by SL molecules.

Constructing a stable and electron-insulating SEI is considered imperative for blocking the side reactions between anodes and electrolytes and enhancing the electrochemical performance of anodes. Although the difference in the XRD peaks (002) is negligible [Supplementary Figure 13], distinct surface morphologies are observed for the MCMB after cycling in the three electrolytes compared with the pristine MCMB [Supplementary Figure 14]. After cycling with BE and LiDFOB-LiBF<sub>4</sub>/SL, some disintegrations and decomposition products can be observed on the surface of MCMB particles, and the thickness of inhomogeneous SEIs formed in the two electrolytes are 7.0 and 5.5 nm, respectively [Figure 4A and B]. Comparatively, intact MCMB particles with integrated and smooth surfaces are observed in the optimized SL-based electrolyte, while the thickness of the homogeneous SEI layer is only 2 nm presented by the HR-TEM [Figure 4C]. In the XPS profiles [Figure 4D and Supplementary Figure 15], B-O (192.0 eV) and LiF (685.0 eV) are detected due to the decomposition of LiDFOB and LiBF<sub>4</sub>. Moreover, the content of sulfur-containing products (RSO<sub>3</sub>Li, Li<sub>2</sub>SO<sub>3</sub> and LiSO<sub>4</sub>) (S-O/B-O peak at 532.6 eV, O 1s) in SEI formed by the FB-containing SL-based electrolyte is significantly less than that of LiDFOB-LiBF<sub>4</sub>/SL, which again proves that FB is reduced together with the dual-salt to form a uniform SEI containing LiF-rich and little sulfur species to suppress the decomposition of SL and promote Li<sup>+</sup> transport.

Commercial LIBs are prone to catching fire and even exploding under abusive conditions, with thermal runaway triggered by violent side reactions at high temperatures (> 60 °C) being the most common and dangerous<sup>[51,52]</sup>. Therefore, it is pragmatic to develop electrolytes with high thermal stability and safety for replacing flammable carbonate-based electrolytes. At 60 °C, the MCMB||NCM811 cells with BE and LiDFOB-LiBF<sub>4</sub>/SL exhibit rapid capacity decay and reach an 80% capacity retention after 126 and 294 cycles, respectively. In sharp comparison, the FB-containing SL-based electrolyte reaches the cutoff criterion of 80% capacity retention after 417 cycles with a high discharge capacity of 149.0 mAh g<sup>-1</sup> [Figure 5A and Supplementary Figure 16]. Figure 5B displays the differential scanning calorimetry (DSC) profiles of the highly charged NCM811 cathodes with the presence of various electrolytes. The designed LSLE exhibits a significant improvement in thermal stability, consequently postponing the onset of the exothermic temperature from 210.3 °C for BE and 227.9 °C for LiDFOB-LiBF<sub>4</sub>/SL to 249.7 °C and decreasing the heat

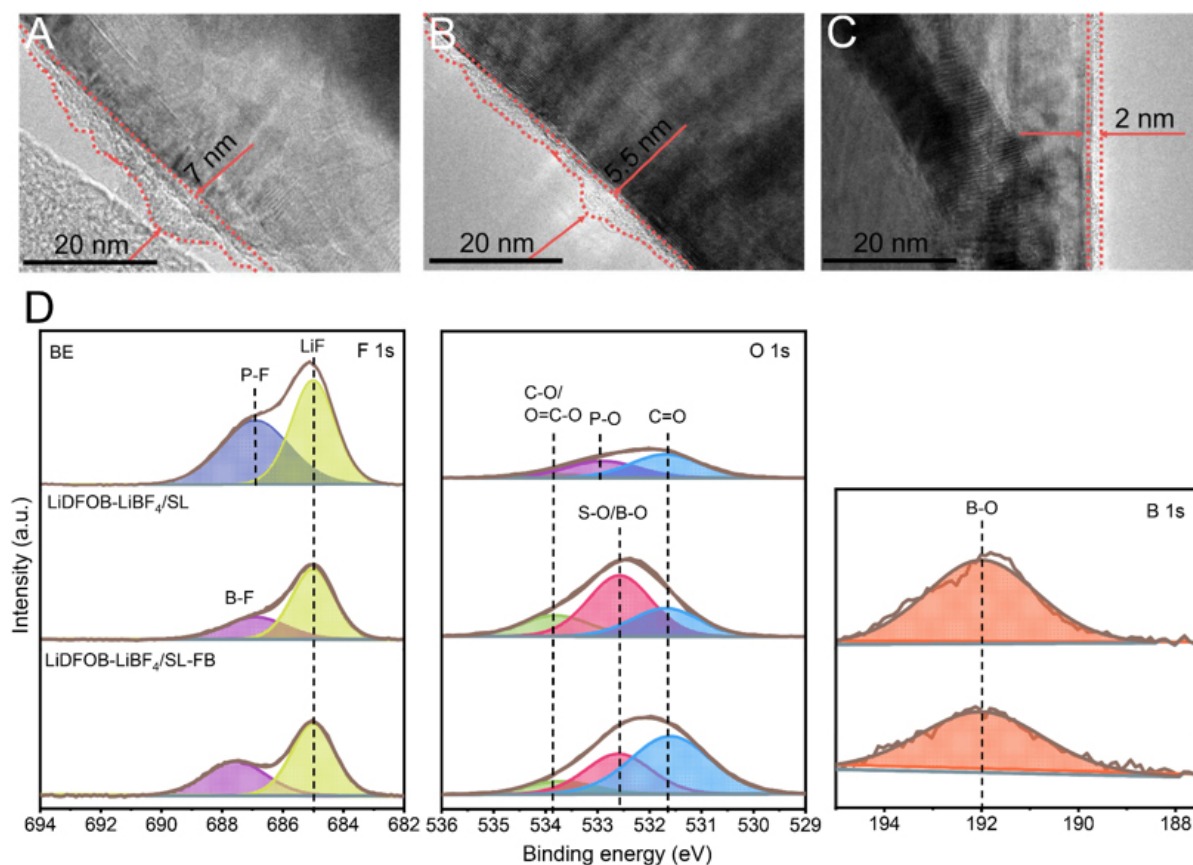


**Figure 4.** Typical HR-TEM images of cycled MCMB electrodes recovered from MCMB||NCM811 full cells after 50 cycles with (A) BE, (B) LiDFOB-LiBF<sub>4</sub>/SL and (C) LiDFOB-LiBF<sub>4</sub>/SL-FB. (D) XPS F 1s, O 1s and B 1s spectra for MCMB anodes recovered from MCMB||NCM811 full cells after 50 cycles with various electrolytes.

generation from 780.6 J g<sup>-1</sup> for BE and 567.1 J g<sup>-1</sup> for LiDFOB-LiBF<sub>4</sub>/SL to 357.6 J g<sup>-1</sup>. Such excellent thermal stability of LiDFOB-LiBF<sub>4</sub>/SL-FB guarantees the stabilization of the interfaces on the aggressive NCM811 cathode and graphite anode. The performance improvement of the optimized SL-based electrolyte is further verified by an industrial 1 Ah artificial graphite (AG)||NCM811 pouch cell [Figure 5C and D]. After two formation cycles at 0.1C, the AG||NCM811 pouch cell with LiDFOB-LiBF<sub>4</sub>/SL-FB enables stable long-term cycling (capacity retention of > 83%) and high Coulombic efficiency (> 99.9%) after 486 cycles. The highly improved stability of the LiDFOB-LiBF<sub>4</sub>/SL-FB electrolyte demonstrates the formation of a stable CEI/SEI on the electrode surfaces, which is beneficial for battery safety and cycle life.

## CONCLUSIONS

In summary, we have demonstrated a FB-containing LSLE system with benign wettability, a wide electrochemical window (> 5.0 V vs. Li/Li<sup>+</sup>), low viscosity and high thermal stability, thus resolving the incompatibility of SL with graphite anodes. It is noteworthy that the synergistic effect of the dual-salt and FB derives interphases with LiF and sulfur-containing species on both the NCM811 cathode and graphite anode, which have a prominent effect in blocking the continual decomposition of SL, facilitating Li<sup>+</sup> transport and mitigating other pernicious side reactions. Therefore, the optimized LSLE system exhibits much better electrochemical performance of the MCMB||NCM811 full cells than commercial carbonate electrolytes, counting for a high capacity retention of 83% after 500 cycles at 25 °C and 82% after 400 cycles at 60 °C. This protocol inspires excellent utility and provides encouraging possibilities for the design of practical electrolyte systems for next-generation high-energy LIBs.

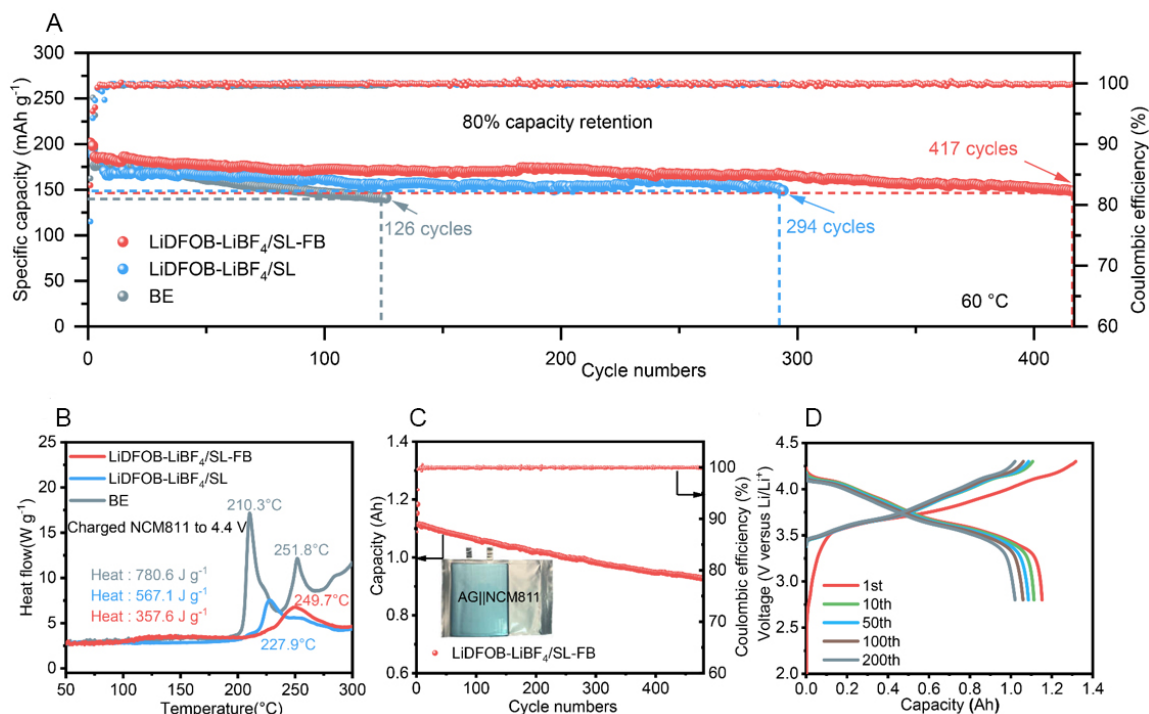


**Figure 5.** (A) Cycling performance and Coulombic efficiency vs. cycle number of MCM811 full cells with various electrolytes at 0.5C between 2.8 and 4.3 V at 60 °C. (B) DSC profiles of charged NCM811 cathode to 4.4 V in Li||NCM811 half-cells with various electrolytes. (C) Cycling performance and Coulombic efficiency vs. cycle number of AG||NCM811 pouch cell using LiDFOB-LiBF<sub>4</sub>/SL-FB under 0.3C within the voltage window of 2.8-4.3 V. (D) Voltage profiles of AG||NCM811 pouch cell with LiDFOB-LiBF<sub>4</sub>/SL-FB.

## DECLARATIONS

### Authors' contributions

Conceived the idea and designed the experiments: Lv L, Fan X

Completed theoretical calculations: Zhang H, Li R

Prepared the electrodes, performed the electrochemical measurements and characterizations: Lv L, Lu D, Qi J, Zhang J

Drafted the manuscript with revisions: Lu D, Yu Y, Zhang S, Deng T, Chen L, Fan X

All authors discussed the results and analysis.

### Availability of data and materials

Not applicable.

### Financial support and sponsorship

This work is supported by the National Natural Science Foundation of China (22072134, 22161142017, and U21A2081), Natural Science Foundation of Zhejiang Province (LZ21B030002), the Fundamental Research Funds for the Zhejiang Provincial Universities (2021XZZX010), the Fundamental Research Funds for the Central Universities (2021FZZX001-09), and "Hundred Talents Program" of Zhejiang University.

### Conflicts of interest

All authors declared that there are no conflicts of interest.

### Ethical approval and consent to participate

Not applicable.

### Consent for publication

Not applicable.

### Copyright

© The Author(s) 2022.

## REFERENCES

1. Whittingham MS. Lithium batteries: 50 years of advances to address the next 20 years of climate issues. *Nano Lett* 2020;20:8435-7. [DOI](#) [PubMed](#)
2. Nitta N, Wu F, Lee JT, Yushin G. Li-ion battery materials: present and future. *Mater Today* 2015;18:252-64. [DOI](#)
3. Goodenough JB, Park KS. The Li-ion rechargeable battery: a perspective. *J Am Chem Soc* 2013;135:1167-76. [DOI](#) [PubMed](#)
4. Zhu C, Sun C, Li R, et al. Anion-diluent pairing for stable high-energy Li metal batteries. *ACS Energy Lett* 2022;7:1338-47. [DOI](#)
5. Etacheri V, Marom R, Elazari R, Salitra G, Aurbach D. Challenges in the development of advanced Li-ion batteries: a review. *Energy Environ Sci* 2011;4:3243. [DOI](#)
6. Li W, Dolocan A, Li J, Xie Q, Manthiram A. Ethylene carbonate-free electrolytes for high-nickel layered oxide cathodes in lithium-ion batteries. *Adv Energy Mater* 2019;9:1901152. [DOI](#)
7. Xu K. Nonaqueous liquid electrolytes for lithium-based rechargeable batteries. *Chem Rev* 2004;104:4303-417. [DOI](#) [PubMed](#)
8. Marom R, Haik O, Aurbach D, Halalay IC. Revisiting LiClO<sub>4</sub> as an electrolyte for rechargeable lithium-ion batteries. *J Electrochem Soc* 2010;157:A972. [DOI](#)
9. Kim J, Lee JG, Kim H, et al. Thermal degradation of solid electrolyte interphase (SEI) layers by phosphorus pentafluoride (PF<sub>5</sub>) attack. *J Electrochem Soc* 2017;164:A2418-25. [DOI](#)
10. Zhan C, Wu T, Lu J, Amine K. Dissolution, migration, and deposition of transition metal ions in Li-ion batteries exemplified by Mn-based cathodes - a critical review. *Energy Environ Sci* 2018;11:243-57. [DOI](#)
11. Xu K. Electrolytes and interphases in Li-ion batteries and beyond. *Chem Rev* 2014;114:11503-618. [DOI](#) [PubMed](#)
12. Li W. Review-an unpredictable hazard in lithium-ion batteries from transition metal ions: dissolution from cathodes, deposition on anodes and elimination strategies. *J Electrochem Soc* 2020;167:090514. [DOI](#)
13. Betz J, Brinkmann J, Nölle R, et al. Cross talk between transition metal cathode and Li metal anode: unraveling its influence on the deposition/dissolution behavior and morphology of lithium. *Adv Energy Mater* 2019;9:1900574. [DOI](#)
14. Fan X, Wang C. High-voltage liquid electrolytes for Li batteries: progress and perspectives. *Chem Soc Rev* 2021;50:10486-566. [DOI](#) [PubMed](#)
15. Kim J, Lee H, Cha H, Yoon M, Park M, Cho J. Prospect and reality of Ni-rich cathode for commercialization. *Adv Energy Mater* 2018;8:1702028. [DOI](#)
16. Zhang N, Li J, Li H, et al. Structural, Electrochemical, and thermal properties of nickel-rich LiNi<sub>x</sub>Mn<sub>y</sub>Co<sub>z</sub>O<sub>2</sub> materials. *Chem Mater* 2018;30:8852-60. [DOI](#)
17. Lu D, Lei X, Weng S, et al. A self-purifying electrolyte enables high energy Li ion batteries. *Energy Environ Sci* 2022;15:3331-42. [DOI](#)
18. Farhat D, Lemordant D, Jacquemin J, Ghamouss F. Alternative electrolytes for Li-ion batteries using glutaronitrile and 2-methylglutaronitrile with lithium bis(trifluoromethanesulfonyl) imide. *J Electrochem Soc* 2019;166:A3487-95. [DOI](#)
19. Zhi H, Xing L, Zheng X, Xu K, Li W. Understanding how nitriles stabilize electrolyte/electrode interface at high voltage. *J Phys Chem Lett* 2017;8:6048-52. [DOI](#) [PubMed](#)
20. Lu D, Xu G, Hu Z, et al. Deciphering the interface of a high-voltage (5 V-Class) Li-ion battery containing additive-assisted sulfolane-based electrolyte. *Small Methods* 2019;3:1900546. [DOI](#)
21. Su C, He M, Redfern PC, Curtiss LA, Shkrob IA, Zhang Z. Oxidatively stable fluorinated sulfone electrolytes for high voltage high energy lithium-ion batteries. *Energy Environ Sci* 2017;10:900-4. [DOI](#)
22. Zhang T, Porcher W, Paillard E. Towards practical sulfolane based electrolytes: choice of Li salt for graphite electrode operation. *J Power Sources* 2018;395:212-20. [DOI](#)
23. Balducci A. Ionic liquids in lithium-ion batteries. In: Kirchner B, Perlt E, editors. *Ionic Liquids II*. Cham: Springer International Publishing; 2018. pp. 1-27. [DOI](#)
24. Fillion JJ, Brennecke JF. Viscosity of ionic liquid-ionic liquid mixtures. *J Chem Eng Data* 2017;62:1884-901. [DOI](#)
25. Nair JR, Colò F, Kazzazi A, et al. Room temperature ionic liquid (RTIL)-based electrolyte cocktails for safe, high working potential

- Li-based polymer batteries. *J Power Sources* 2019;412:398-407. DOI
26. Chen S, Yu Z, Gordin ML, Yi R, Song J, Wang D. A fluorinated ether electrolyte enabled high performance prelithiated graphite/sulfur batteries. *ACS Appl Mater Interfaces* 2017;9:6959-66. DOI PubMed
  27. Suo L, Xue W, Gobet M, et al. Fluorine-donating electrolytes enable highly reversible 5-V-class Li metal batteries. *Proc Natl Acad Sci USA* 2018;115:1156-61. DOI PubMed PMC
  28. Fan X, Ji X, Chen L, et al. All-temperature batteries enabled by fluorinated electrolytes with non-polar solvents. *Nat Energy* 2019;4:882-90. DOI
  29. Chen J, Fan X, Li Q, et al. Electrolyte design for LiF-rich solid-electrolyte interfaces to enable high-performance micro-sized alloy anodes for batteries. *Nat Energy* 2020;5:386-97. DOI
  30. Fan X, Chen L, Borodin O, et al. Non-flammable electrolyte enables Li-metal batteries with aggressive cathode chemistries. *Nat Nanotechnol* 2018;13:715-22. DOI PubMed
  31. Zhang T, Paillard E. Recent advances toward high voltage, EC-free electrolytes for graphite-based Li-ion battery. *Front Chem Sci Eng* 2018;12:577-91. DOI
  32. Alvarado J, Schroeder MA, Zhang M, et al. A carbonate-free, sulfone-based electrolyte for high-voltage Li-ion batteries. *Mater Today* 2018;21:341-53. DOI
  33. Ko S, Yamada Y, Yamada A. An overlooked issue for high-voltage Li-ion batteries: Suppressing the intercalation of anions into conductive carbon. *Joule* 2021;5:998-1009. DOI
  34. Fu J, Ji X, Chen J, et al. Lithium nitrate regulated sulfone electrolytes for lithium metal batteries. *Angew Chem Int Ed Engl* 2020;59:22194-201. DOI PubMed
  35. Zygadlo-monikowska E, Florjańczyk Z, Kubisa P, et al. Mixture of LiBF<sub>4</sub> and lithium difluoro(oxalato)borate for application as a new electrolyte for lithium-ion batteries. *J Power Sources* 2010;195:6202-6. DOI
  36. Zhou H, Xiao K, Li J. Lithium difluoro(oxalato)borate and LiBF<sub>4</sub> blend salts electrolyte for LiNi<sub>0.5</sub>Mn<sub>1.5</sub>O<sub>4</sub> cathode material. *J Power Sources* 2016;302:274-82. DOI
  37. Zuo X, Fan C, Liu J, Xiao X, Wu J, Nan J. Lithium tetrafluoroborate as an electrolyte additive to improve the high voltage performance of lithium-ion battery. *J Electrochem Soc* 2013;160:A1199-204. DOI
  38. Zhou H, Xiao D, Yin C, Yang Z, Xiao K, Li J. Enhanced performance of the electrolytes based on sulfolane and lithium difluoro(oxalato)borate with enhanced interfacial stability for LiNi<sub>0.5</sub>Mn<sub>1.5</sub>O<sub>4</sub> cathode. *J Electrochem* 2018;808:293-302. DOI
  39. Bian X, Ge S, Pang Q, et al. A novel lithium difluoro(oxalato) borate and lithium hexafluoride phosphate dual-salt electrolyte for Li-excess layered cathode material. *J Alloys Compd* 2018;736:136-42. DOI
  40. Hu M, Wei J, Xing L, Zhou Z. Effect of lithium difluoro(oxalato)borate (LiDFOB) additive on the performance of high-voltage lithium-ion batteries. *J Appl Electrochem* 2012;42:291-6. DOI
  41. Cha J, Han J, Hwang J, Cho J, Choi N. Mechanisms for electrochemical performance enhancement by the salt-type electrolyte additive, lithium difluoro(oxalato)borate, in high-voltage lithium-ion batteries. *J Power Sources* 2017;357:97-106. DOI
  42. Jiang Z, Zeng Z, Liang X, et al. Fluorobenzene, a low-density, economical, and bifunctional hydrocarbon cosolvent for practical lithium metal batteries. *Adv Funct Mater* 2021;31:2005991. DOI
  43. Kresse G, Furthmüller J. Efficient iterative schemes for ab initio total-energy calculations using a plane-wave basis set. *Phys Rev B Condens Matter* 1996;54:11169-86. DOI PubMed
  44. Kresse G. Ab initio molecular dynamics for liquid metals. *J Non-Cryst Solids* 1995;192-193:222-229. DOI
  45. Kresse G, Hafner J. Ab initio molecular-dynamics simulation of the liquid-metal-amorphous-semiconductor transition in germanium. *Phys Rev B Condens Matter* 1994;49:14251-69. DOI PubMed
  46. Liang JY, Zhang XD, Zhang Y, et al. Cooperative shielding of Bi-electrodes via in situ amorphous electrode-electrolyte interphases for practical high-energy lithium-metal batteries. *J Am Chem Soc* 2021;143:16768-76. DOI PubMed
  47. Bai P, Ji X, Zhang J, et al. Formation of LiF-rich cathode-electrolyte interphase by electrolyte reduction. *Angew Chem Int Ed Engl* 2022;61:e202202731. DOI PubMed PMC
  48. Gaberšček M. Understanding Li-based battery materials via electrochemical impedance spectroscopy. *Nat Commun* 2021;12:6513. DOI PubMed PMC
  49. Bolloju S, Chiou C, Vikramaditya T, Lee J. (Pentafluorophenyl)diphenylphosphine as a dual-functional electrolyte additive for LiNi<sub>0.5</sub>Mn<sub>1.5</sub>O<sub>4</sub> cathodes in high-voltage lithium-ion batteries. *Electrochim Acta* 2019;299:663-71. DOI
  50. Martha SK, Nanda J, Veith GM, Dudney NJ. Surface studies of high voltage lithium rich composition: Li<sub>1.2</sub>Mn<sub>0.525</sub>Ni<sub>0.175</sub>Co<sub>0.1</sub>O<sub>2</sub>. *J Power Sources* 2012;216:179-86. DOI
  51. Xiong DJ, Petibon R, Nie M, Ma L, Xia J, Dahn JR. Interactions between positive and negative electrodes in Li-ion cells operated at high temperature and high voltage. *J Electrochem Soc* 2016;163:A546-51. DOI
  52. He M, Boulet-roblin L, Borel P, et al. Effects of solvent, lithium salt, and temperature on stability of carbonate-based electrolytes for 5.0 V LiNi<sub>0.5</sub>Mn<sub>1.5</sub>O<sub>4</sub> electrodes. *J Electrochem Soc* 2016;163:A83-9. DOI